Published in final edited form as:
Science. 2010 August 27; 329(5995): 1038–1043. doi:10.1126/science.1187433.

Atomic structure of human adenovirus by cryoEM reveals interactions among protein networks

Hongrong Liu[1,2,3], **Lei Jin**[1,2], **Sok Boon S. Koh**[4], **Ivo Atanasov**[2], **Stan Schein**[2,5,6], **Lily Wu**[2,4], and **Z Hong Zhou**[1,2,*]

[1] Department of Microbiology, Immunology and Molecular Genetics, University of California, Los Angeles (UCLA), Los Angeles, CA 90095-7364, USA

[2] California NanoSystems Institute, UCLA, Los Angeles, CA 90095-7151, USA

[3] Institute of Modern physics, Xiangtan University, Xiangtan, Hunan 411105, China

[4] Department of Molecular & Medical Pharmacology, Institute of Molecular Medicine (IMED), UCLA School of Medicine, Los Angeles, CA 90095-1735, USA

[5] Department of Psychology, UCLA, Los Angeles, CA 90095-1563, USA

[6] Brain Research Institute, UCLA, Los Angeles, CA 90095-1761, USA

Abstract

Construction of a complex virus may involve a hierarchy of assembly elements. Here, we report the structure of the whole human adenovirus virion at 3.6Å resolution by cryo-electron microscopy, revealing *in situ* atomic models of three minor capsid proteins (IIIa, VIII and IX), extensions of the major (penton base and hexon) capsid proteins, and interactions within three protein-protein networks. One network is mediated by protein IIIa within Group-of-Six (GOS) tiles – a penton base and its five surrounding hexons – at vertices. Another is mediated by ropes (protein IX) that lash hexons together to form Group-of-Nine (GON) tiles and bind GONs to GONs. The third, mediated by IIIa and VIII, binds each GOS to five surrounding GONs. Optimization of adenovirus for cancer and gene therapy could target these networks.

Human adenovirus (Ad) causes acute respiratory, gastrointestinal, and ocular infections as well as fulminant infections among children and immuno-compromised individuals, and engineered versions are used for gene therapy and vaccines against cancer and other diseases (1-4). It is among the largest (~920Å diameter) and most complex (~150MDa), non-enveloped double-stranded DNA (dsDNA) viruses (5). Its icosahedral capsid shell (Fig. 1) is composed of three major proteins: 240 hexon trimers ('hexons'), each in the shape of a hexagon, 12 penton base pentamers ('penton base'), each in the shape of a pentagon, 12 penton-base associated fiber trimers ('fibers') and four minor proteins (IIIa, VI, VIII and IX) (table S1) (5-7). The genome core inside the capsid is composed of the DNA, five additional proteins (V, VII, μ, IVa2, terminal protein), and viral protease (8). We sought to characterize the logic and details of the interactions responsible for assembly and stabilization of the virion.

Crystal structures (~3Å) are available for the isolated hexon (9, 10), penton base (11) and fiber (12). Cryo-electron microscopy (cryoEM) structures are available for the intact virion

[*]**Correspondence to**Hong.Zhou@ucla.edu. Phone 310.983.1033.

Supporting Online Material www.sciencemag.org Materials and Methods Supporting Text Figs. S1 to S10 Tables S1 to S5 Movie S1 to S10

(7, 13-17) – including the minor proteins VIII and IIIa on the inner surface of the capsid and IX on the outer surface – but at a resolution (6Å) (15) that does not permit characterization of interactions among the proteins. Here, we report a 3.6Å resolution structure of human adenovirus type 5 (Ad5) by cryoEM single-particle analysis, enabling us to construct atomic models for these three minor proteins and resolve critical regions of the hexon and penton base not seen by x-ray crystallography. These models reveal networks of interactions mediated by minor proteins IIIa, VIII and IX that stabilize two large systems of tiles – on each facet a Group of Nine (GON) capsomers (6, 18-20) and at each vertex a Group of Six (GOS) capsomers – and hold those tiles together.

Overall structure of the virion

We reconstructed the three-dimensional (3D) structure (density map) of Ad5 (Fig. 1A; movies S1, S2) from 31,815 individual particle images in 1350 films using IMIRS software package (21) (see Materials and methods in SOM) (22). The effective resolution of our structure, 3.6Å, is estimated by the reference-based Fourier shell correlation (FSC) coefficient (23) (Fig. S1). Representative α-helix (Fig. 1C; movie S3) and β-strand density maps (Fig. S2; movie S4) from the hexon protein (movie S5) are consistent with this estimate.

The 240 quasi-equivalent hexons are classified as H1, H2, H3 and H4 according to their location within each facet of the pseudo T=25 icosahedral capsid (6) (Fig. 1B). The 12 penton bases occupy the 12 vertices of the icosahedron (Fig. 1A,B), and each of the 12 fiber trimers associates with a penton base. The densities of hexons, penton bases, fibers, and the four minor proteins (IIIa, VIII, VI, and IX) are individually colored in Figure 1B and movie S2. Minor protein IX (Fig. 1B, upper panel) is inlaid in the outer surface of the capsid – not on the outer surface itself but halfway down the hexon (15, 16) (side view in the upper left inset of Fig. 1B). By contrast, minor proteins IIIa and VIII sit on the inner surface (Fig. 1B, lower panel) underneath the boundaries of penton bases and hexons (side view in the lower right inset of Fig. 1B) (15). Protein VI is also located beneath hexons, as indicated by previous cryoEM structures, in a cavity on the inner surface of each hexon (15, 24). Our result is consistent with this observation, but perhaps due to random occupancy (~360 copies among 720 hexon monomers), the cryoEM density is weak. The copy numbers and resolved amino acids of these capsid proteins are summarized in table S1.

Protein IIIa

Monomers of protein IIIa, underneath the penton base and peripentonal (H1) hexons, are arranged around the 5-fold axis (Fig. 2A). We resolve the structure of aa 7-300 of protein IIIa. The remainder of the protein (aa 301-585) is not visible, implying flexibility. The resolved structure is predominantly helical (Fig. 2B), with only one 3-stranded β sheet (Fig. S3). It has the shape of a seahorse (Fig. 2B and movie S6) and can be divided into four domains according to their interactions with other proteins (Fig. 2B). We can visualize densities associated with side chain of ~85% of the amino acids (Fig. S3), but not all of these densities are sufficiently distinctive for us to identify amino acids. Therefore, we use amino acids that are large and distinctive (table S2) as ‘landmarks’ to obtain accurate registration of amino acids in our atomic model. Construction of the protein IIIa atomic model allows us to describe interactions with other proteins by identifying amino acids with a visible density at the site of side-chain contacts (SOM; proposed details of 9 sites of interactions in table S3A.). For example, the GOS-glue domain, the tail of the seahorse, interacts with a penton-base monomer (Fig. 2A, lower right inset), an adjacent protein IIIa (same inset), and two peripentonal hexons, thus binding the penton base to neighboring

peripentonal hexons. The VIII-binding domain, the neck of the seahorse, interacts with protein VIII (Fig. 2A, upper right inset) to bind peripentonal hexons to hexons farther away.

Protein VIII

Monomers of protein VIII, also located on the inner capsid surface, are arranged around both 5-fold and 3-fold axes (Fig. 2A). Each monomer is organized into an extended conformation with three domains, head, neck, and body (Fig. 2C). Our density map and the resulting model of the head domain are in good agreement with previous mass spectrometry data showing that protein VIII is cleaved at two positions during viral maturation, G110 and R159, (Fig. 2C, lower inset), causing the middle segment (aa 111-158) to be shed from the mature capsid (25). As with protein IIIa, we can visualize densities associated with side chains of ~85% of the amino acids (Fig. S4, and we use bulky amino acids (table S2) as landmarks to build our atomic model (Fig. S4 and movie S7). Similarly, we identify 13 sites of interactions – each characterized by visible densities at the sites of side-chain contacts - for each protein VIII with other proteins (SOM; proposed details on interactions in table S3B). For example, every copy of protein VIII interacts with four hexons, two on either side of its body, one to the side of its neck, and one to the side of its head (Fig. 2A, center). The large body domain includes three anti-parallel β strands that interact with protein IIIa (Fig. 2A, top right inset). In addition, each of the β strands in the head and body domains join the β sheets of the VC region of two hexons via β-strand augmentation (Fig. 2A, top insets).

Protein IX

The protein IX network is best viewed from the outside (multi-colored in Fig. 3A, center). Each monomer (Fig. 3B) has an N-terminal domain (~50Å long), a rope domain (~70Å), and a helix-bundle domain with a long 12-turn helix (~65Å), all joined by loops. We could visualize the densities of side-chain of ~85% of the amino acids in the N-terminal domain and ~70% in the helix-bundle domain (Fig. S5A,B). As above, we use bulky amino acids (table S2) as landmarks to obtain accurate registration of amino acids in our atomic model for these two domains. In addition, we describe protein IX's interactions with other proteins by identifying either visible densities at the sites of side-chain contacts (for the N-terminal and helix-bundle domains) or by close proximity (for the rope domains) (SOM; proposed details of 6 sites of interactions in table S3C).

At the N-termini of three protein IX monomers, the N-joint regions (Fig.3B, blue) form a trimeric joint (Fig. 3A, upper left inset, Fig. S5C and movie S8). The three contributing monomers radiate from this joint, either three yellow monomers or a red, a green and a blue (Fig. 3A, center). Four of these N-joints are located in each facet, one at the 3-fold axis (yellow in Fig. 3A) and three at local-3-fold axes (each with red, green, and blue monomers in Fig. 3A). The N-joint is tied by a hydrophobic core that includes three tyrosines and three leucines (Fig. 3A, upper insets).

At the C-terminus of a protein IX, four helix-bundle domains coil together to form a ~65Å long four-helix bundle (Fig. 3A, right insets; Fig. S5D and movie S9). These four-helix bundles, three in each facet, are centered on three local 2-fold positions inside the three edges of a facet. The amino acid sequence in the helix-bundle domain of protein IX shows a heptad-repeat motif with the hydrophobic Leu in the *d* position (Leucine zipper: L100, L107, L114 and L121), typical of a helix bundle. Indeed, there are additional hydrophobic leucines and valines in the helix-bundle domain, specifically L103, L110, V117, L124, V128, and L131 (table S4).

Three of the helices (blue, yellow and green) of a four-helix bundle come from the same facet of the capsid and traverse the same distance, two hexagon edges (eac~60Å), before

joining at the *base* of the bundle (center of Fig. 3A; see also the Section "Interaction networks" below). These would run in parallel with each other. However, the fourth helix (red) comes from a neighboring facet, reaches the *tip* of the helix bundle after traversing the standard two hexagon edges, joins the bundle there, and continues to the base of the helix bundle (black arrows in Fig. S5E,F). Inspired by Fig. 4 in ref. (15), this arrangement, with the red helix running anti-parallel to the other three, was already demonstrated by use of peptide-tagged recombinant protein IX (26).

Identification of amino-acid side chains among the four helices (Fig. S5D, table S2) and visualization of the densities of the rope domains of the four proteins IX in an asymmetric unit (movie S10) confirm this unusual arrangement with three parallel helices and one anti-parallel helix. Indeed, the hydrophobic leucines and valines listed above create a ladder of hydrophobic interactions between these parallel and anti-parallel helix-bundle domains (table S4) to create a hydrophobic core (Fig. 3A, upper right and lower right insets). This arrangement would tack down both ends of the helix bundle and hold the bundle rigidly in place, perhaps explaining why the helix bundle is well resolved in structural studies.

Although filtering to low resolution reveals all of the parts of all four copies of protein IX (Fig. S5E,F and movie S10), our high-resolution structure shows clearly the entirety of just the blue copy (Fig. S5A,B). Therefore, we use flexible fitting of the blue rope domain to model the green, yellow and red rope domains in the center of Figure 3A. Even for the blue copy, amino acid registration for the rope domain is uncertain due to the relatively low density of that domain (Fig. S5A,E). With that caution in mind, we have nonetheless built an atomic model of all three domains of the blue copy of protein IX. For the red, green and yellow copies, we have built atomic models of only their N-terminal and helix bundle domains.

Major capsid proteins and conformational adaptability

Derived from the cryoEM density map of the whole virion, our atomic models of the penton-base and hexon proteins (Fig. 4A,B, red ribbons) are in excellent agreement with those from x-ray crystallography (9-11). However, our models reveal features not seen in the crystal structures as well as many *in situ* interactions absent from crystal structures of isolated proteins. For example, at the N-terminus of each penton base monomer we see amino acids 37-51 (blue 'N-arm' in Fig. 4A). This string of amino acids interacts with two adjacent IIIa proteins (Fig. 2A, lower right inset; model and densities in Fig. S6; table S3A) and then turns inward to connect with the genome core, thus anchoring the penton base.

We also see an N-terminal extension (aa 2-7) and a C-terminal extension (aa 944-950) of the hexon. With four types of hexon (H1-H4) in an asymmetric unit, there are 12 hexon monomers (Fig. S7A), but depending on the location of the subunit and adapting to its interaction with neighboring proteins (see legend of Fig. 4C), the N-terminal extension (Fig. 4C) shows just five different conformations for its short stretch of amino acids. Some of these conformations interact with minor proteins IIIa and VIII on the inner surface (tables S3A,B), others with neither. Likewise, the C-terminal extension (aa 944-950 in Figs. 4D and S8A) shows different conformations, six in this case. The first three, like the C-terminal extension type *a* (Fig. S8B), interact with protein VIII; the last three do not.

In addition, at the top of the hexon in our cryoEM model we see four loops (aa 251-256, 271-278, 431-436, 443-444) (Fig. 4B, blue ribbons and labels). The first three are within the hypervariable regions HVR4, HVR5 and HVR7 that are important for type-specific immunogenicity (10). The one loop (aa 251-256) in the H4 hexon monomer interacts with the tip of four-helix bundle of protein IX and anchors the latter in the valley between two hexons.

Finally, our 3.6Å resolution structure shows the amino acids involved in hexon-hexon and hexon-penton base interactions by identifying amino-acid residues that are within 7Å distance (Fig. S7 and proposed details of interactions in table S5). Based on the scarcity of visible side-chain contact densities, we suggest that these interactions are generally weaker (like the one shown in Fig. S7B) than those between the major and minor proteins. Although these interactions cannot be seen in the crystal structures of the individual proteins, they are largely in agreement with predictions based on fitting the crystal structures to these proteins in their native packing, as revealed in 10Å cryoEM maps of the whole virion [table 1 in ref. (14)].

Interactions with the genome core

Our map also revealed interactions of two kinds between capsid shell proteins and the genome core, indicating a role for capsid proteins in genome packaging. The first kind is the N-arm of the penton base, extending to the genome core (Fig. S9A-C), consistent with the report that the penton base can bind core protein V (27). The second kind is a density underneath and near protein IIIa (Fig. S9D), which looks like a rod at low resolution and has the characteristic features of a helix at high resolution. According to its site and copy number, 60 per virion, this rod density is likely to be part of the C-terminus of protein IIIa, consistent with the ability of protein IIIa also to bind core protein V (17, 28).

Prior reports show that protein VI binds hexons (29) and core protein V (30), and its C-terminus activates the virion protease that cleaves multiple precursor proteins, required for virion maturation and infectivity (31). We find protein VI in the cavity on the underside of the hexon, consistent with these observations.

Interaction networks among minor and major proteins

Using detergent, Smith et al (18) obtained dissociation fragments that became known as GONs – Groups of Nine (20) hexons – one in each of the 20 facets (6). Following that example, we call the one penton base pentamer and its five peripentonal hexons a GOS – a Group of Six capsomers – each centered on a vertex (Fig. 5A schematic).

As shown in the sphere in Figure 2A and in the Figure 5A schematic, five copies of protein IIIa monomer (red) on the *inner* surface of the capsid form a network centered on a penton base. This network appears to hold together the penton base and peripentonal hexons to form a GOS, with many contacts between penton base and peripentonal hexons and between peripentonal-hexon neighbors (Fig. S10A and Table S3A).

From the network point of view, the protein VIII molecule (blue) on the inner surface of the capsid has three kinds of interactions (Fig. 5A schematic, Fig. S10A, and Table S3B). First, its head and neck domains bind neighboring hexons within each GON. Second, its body domain binds neighboring GONs to each other at a local 2-fold position (*i.e.*, the SS interface between H3 and H2 hexons in Fig. S7A). Third, its body domain joins GON hexons and GOS hexons at another local 2-fold position (*i.e.*, the SS interface between H4 and H1 hexons in Fig. S7A). Indeed, this last type of interaction appears to be the main interaction between GON and GOS tiles.

Protein IX on the *outer* surface of the capsid forms a network that lines the boundaries between hexons, bonds extensively with them, lashes them together into GONs, and binds GONs to GONs (Fig. 5B). Coextensive with GONs, protein IX essentially avoids GOS tiles, with only one monomer – the red one – having just one interaction site with H1 hexon protein (#5 in Table S3C). Detergent treatment dissociates adenovirus into GONs and GOS capsomers (18). We suppose that this dissociation is the result of disruption of the

hydrophobic cores within the three four-helix bundles situated at local 2-fold positions (TT interfaces between H2 and H4 hexons in Fig. S7A) at the edges of each GON (Fig. 5B, table S5). Moreover, dissociation of a protein IX-deletion mutant virus produces isolated hexon and penton base capsomers but no GONs (32).

The schematic (Fig. 5B) also illustrates the argument that the yellow, blue and green protein IX monomers traverse two hexagon edges before reaching the base of the four-helix bundle, whereas the red monomer traverses two hexagon edges before reaching the tip of the four-helix bundle. The blue protein IX monomer extends along the sides of just one hexon (H4), whereas the others must be more flexible in crossing the valley between two different hexons, perhaps explaining why the density of the blue one is best resolved. Indeed, the four monomers take different combinations of turns at the beginning and at the end of their rope domain, specifically, the parallel blue turns left and left, the parallel yellow turns right and left, the parallel green turns left and right in Fig. 5B, consistent with the diagram in Fig. 4D of ref. (15), and the anti-parallel red from the neighboring GON turns left and left. In addition, the green helix domain crosses over the other three and interacts with a hexon (H4) (Fig. 5B and table S3C).

Discussion

Many double-stranded DNA viruses, including some bacteriophages and herpesviruses, assemble a protein capsid first, followed by motor-driven insertion of genomic DNA through a portal complex at one of the 12 vertices into the preformed capsid (33, 34). Indeed, a recent study suggests the presence in adenovirus of a homolog of the bacteriophage portal protein (35). Moreover, empty capsid particles and normal-size particles with a fraction of the normal DNA have been detected (36). Therefore, the size of the virion is likely to be determined by its capsid components, probably the assembly of GON and GOS tiles, which depend primarily on interactions between major and minor proteins (Fig. 5). For example, in the absence of protein IX – which may act like the 'tape-measure' protein P30 in bacteriophage PRD1 (37, 38) – the adenovirus virion can accommodate a slightly larger than normal genome (39). If the protein IX network, with several domains that are tied at both ends – the N-joint at one and the four-helix bundle at the other – is under tension, its elastic cables working in opposition to the outward force from the core stuffed with enough DNA (40) may be essential to the stability of the virus. Indeed, adenovirus without protein IX has poor thermostability (32).

Our atomic structures have enabled us to identify the amino acids responsible for interactions among the minor and major proteins in the virion (tables S3-S5). By genetic engineering, these amino acids could be systematically manipulated to generate more stable, less stable, or temperature-sensitive particles and conceivably larger capsids. Such larger capsids might permit an increase in the payload of genes carried by an engineered adenovirus for cancer and gene therapy. In addition, our atomic model of the whole virion has revealed which amino acids of protein IX, the hexon, and the penton-base are exposed on the outer surface. These amino acids could serve as targets for genetic engineering to modulate tissue targeting (41). Finally, insofar as adenovirus causes illness, especially among young children and immuno-compromised adults, it should be possible to rationally design drugs to target those binding sites.

Supplementary Material

Refer to Web version on PubMed Central for supplementary material.

Acknowledgments

We thank Arnold Berk for advice; Wong H. Hui for imaging, Dr. Chae-Ok Yun and Oh-Joon Kwon for providing the Ad-ΔE1B19/55 virus sample, and Xing Zhang and Peng Ge for discussion. This project is supported in part by grants from the National Institutes of Health (GM071940 and AI069015 to ZHZ) and (CA101904 to LW). We acknowledge use of facilities at the Electron Imaging Center for NanoMachines supported in part by NIH (1S10RR23057). S.B.K.was supported by CDMRP W81XWH-06-1-055 predoctoral training program. HL thanks the National Natural Scientific Foundation of China for support (10874144). Our structure and atomic model have been deposited in the EM Data Bank and the Protein Data Bank with accession numbers EMD-5172 and 3IYN, respectively.

References

1. Roberts DM, et al. Hexon-chimaeric adenovirus serotype 5 vectors circumvent pre-existing anti-vector immunity. Nature. 2006; 441:239. [PubMed: 16625206]
2. Everts M, Curiel DT. Transductional targeting of adenoviral cancer gene therapy. Curr. Gene Ther. 2004; 4:337. [PubMed: 15384947]
3. Tatsis N, Ertl HCJ. Adenoviruses as vaccine vectors. Mol. Ther. 2004; 10:616. [PubMed: 15451446]
4. Waddington SN, et al. Adenovirus serotype 5 hexon mediates liver gene transfer. Cell. 2008; 132:397. [PubMed: 18267072]
5. Berk, AJ. Adenoviridae: The Viruses and Their Replication.. In: Knipe, DM.; Howley, PM., editors. Fields Virology. Vol. II. Lippincott Williams & Wilkins Philadelphia; Pennsylvania: 2007. p. 2356-2395.
6. Burnett RM. The structure of adenovirus capsid II. The packing symmetry of hexon and its implications for viral architecture. J. Mol. Biol. 1985; 185:125. [PubMed: 4046035]
7. Stewart PL, Fuller SD, Burnett RM. Difference imaging of adenovirus: bridging the resolution gap between x-ray crystallography and electron microscopy. EMBO J. 1993; 12:2589. [PubMed: 8334984]
8. Russell WC. Adenoviruses: update on structure and function. J. Gen. Virol. 2009; 90:1. [PubMed: 19088268]
9. Roberts MM, White JL, Grütter MG, Burnett RM. Three-dimensional structure of the adenovirus major coat protein hexon. Science. 1986; 232:1148. [PubMed: 3704642]
10. Rux JJ, Kuser PR, Burnett RM. Structural and phylogenetic analysis of adenovirus hexons by use of high-resolution X-ray crystallographic, molecular modeling, and sequence-based methods. J. Virol. 2003; 77:9553. [PubMed: 12915569]
11. Zubieta C, Schoehn G, Chroboczek J, Cusack S. The structure of the human adenovirus 2 penton. Mol. Cell. 2005; 17:121. [PubMed: 15629723]
12. van Raaij MJ, Mitraki A, Lavigne G, Cusack S. A triple β-spiral in the adenovirus fibre shaft reveals a new structural motif for a fibrous protein. Nature. 1999; 401:935. [PubMed: 10553913]
13. Stewart PL, Burnett RM, Cyrklaff M, Fuller SD. Image reconstruction reveals the complex molecular organization of adenovirus. Cell. 1991; 67:145. [PubMed: 1913814]
14. Fabry CM, et al. A quasi-atomic model of human adenovirus type 5 capsid. EMBO J. 2005; 24:1645. [PubMed: 15861131]
15. Saban SD, Silvestry M, Nemerow GR, Stewart PL. Visualization of α-helices in a 6-Ångstrom resolution cryoelectron microscopy structure of adenovirus allows refinement of capsid protein assignments. J. Virol. 2006; 80:12049. [PubMed: 17005667]
16. Marsh MP, et al. Cryoelectron microscopy of protein IX-modified adenoviruses suggests a new position for the C terminus of protein IX. J. Virol. 2006; 80:11881. [PubMed: 16987967]
17. Silvestry M, et al. Cryo-electron microscopy structure of adenovirus type 2 temperature-sensitive mutant 1 reveals insight into the cell entry defect. J. Virol. 2009; 83:7375. [PubMed: 19458007]
18. Smith KO, Gehle WD, Trousdale MD. Architecture of the adenovirus capsid. J. Bact. 1965; 90:254. [PubMed: 16562026]
19. Crowther RA, Franklin RM. The structure of the groups of nine hexons from adenovirus. J. Mol. Biol. 1972; 68:181. [PubMed: 5050362]

20. Laver WG, Pereira HG, Russell WC, Valentine RC. Isolation of an internal component from adenovirus type 5. J. Mol. Biol. 1968; 37:379. [PubMed: 5719215]
21. Liang Y, Ke EY, Zhou ZH. IMIRS: a high-resolution 3D reconstruction package integrated with a relational image database. J. Struct. Biol. 2002; 137:292. [PubMed: 12096897]
22. Materials and methods are available as supporting material on Science Online.
23. Rosenthal PB, Henderson R. Optimal determination of particle orientation, absolute hand, and contrast loss in single-particle electron cryomicroscopy. J. Mol. Biol. 2003; 333:721. [PubMed: 14568533]
24. Pérez-Berná AJ, et al. Structure and uncoating of immature adenovirus. J. Mol. Biol. 2009; 392:547. [PubMed: 19563809]
25. Lehmberg E, et al. Reversed-phase high-performance liquid chromatographic assay for the adenovirus type 5 proteome. J. Chromatogr. B. 1999; 732:411.
26. Fabry CMS, et al. The C-terminal domains of adenovirus serotype 5 protein IX assemble into an antiparallel structure on the facets of the capsid. J. Virol. 2009; 83:1135. [PubMed: 19004948]
27. Everitt E, Lutter L, Philipson L. Structural proteins of adenoviruses : XII. Location and neighbor relationship among proteins of adenovirion type 2 as revealed by enzymatic lodination, immunoprecipitation and chemical cross-linking. Virology. 1975; 67:197. [PubMed: 808902]
28. Boudin M, D'Halluin JC, Cousin C, Boulanger P. Human adenovirus type 2 protein IIIa. II. Maturation and encapsidation. Virology. 1980; 101:144. [PubMed: 7355575]
29. Wiethoff CM, Wodrich H, Gerace L, Nemerow GR. Adenovirus protein VI mediates membrane disruption following capsid disassembly. J. Virol. 2005; 79:1992. [PubMed: 15681401]
30. Matthews DA, Russell WC. Adenovirus core protein V is delivered by the invading virus to the nucleus of the infected cell and later in infection is associated with nucleoli. J. Gen. Virol. 1998; 79:1671. [PubMed: 9680130]
31. McGrath WJ, Ding J, Didwania A, Sweet RM, Mangel WF. Crystallographic structure at 1.6-Å resolution of the human adenovirus proteinase in a covalent complex with its 11-amino-acid peptide cofactor: insights on a new fold. Biochim. Biophys. Acta. 2003; 1648:1. [PubMed: 12758141]
32. Colby WW, Shenk T. Adenovirus type 5 virions can be assembled in vivo in the absence of detectable polypeptide IX. J. Virol. 1981; 39:977. [PubMed: 7288921]
33. Jiang W, et al. Structure of epsilon15 bacteriophage reveals genome organization and DNA packaging/injection apparatus. Nature. 2006; 439:612. [PubMed: 16452981]
34. Deng B, O'Connor CM, Kedes DH, Zhou ZH. Direct visualization of the putative portal in the Kaposi's sarcoma-associated herpesvirus capsid by cryoelectron tomography. J Virol. 2007; 81:3640. [PubMed: 17215290]
35. Ostapchuk P, Hearing P. Control of adenovirus packaging. J. Cell Biochem. 2005; 96:25. [PubMed: 15988756]
36. Prage L, Höglund S, Philipson L. Structural proteins of adenoviruses VIII. characterization of incomplete particles of adenovirus type 3. Virology. 1972; 49:745. [PubMed: 5072634]
37. Cockburn JJB, et al. Membrane structure and interactions with protein and DNA in bacteriophage PRD1. Nature. 2004; 432:122. [PubMed: 15525993]
38. Abrescia NGA, et al. Insights into assembly from structural analysis of bacteriophage PRD1. Nature. 2004; 432:68. [PubMed: 15525981]
39. Sargent K, Ng P, Evelegh C, Graham F, Parks R. Development of a size-restricted pIX-deleted helper virus for amplification of helper-dependent adenovirus vectors. Gene Therapy. 2004; 11:504. [PubMed: 14999222]
40. Smith AC, Poulin KL, Parks RJ. DNA genome size affects the stability of the adenovirus virion. J. Virol. 2009; 83:2025. [PubMed: 19036812]
41. Yan M, et al. A novel intracellular protein delivery platform based on single-protein nanocapsules. Nature nanotech. 2010; 5:48.

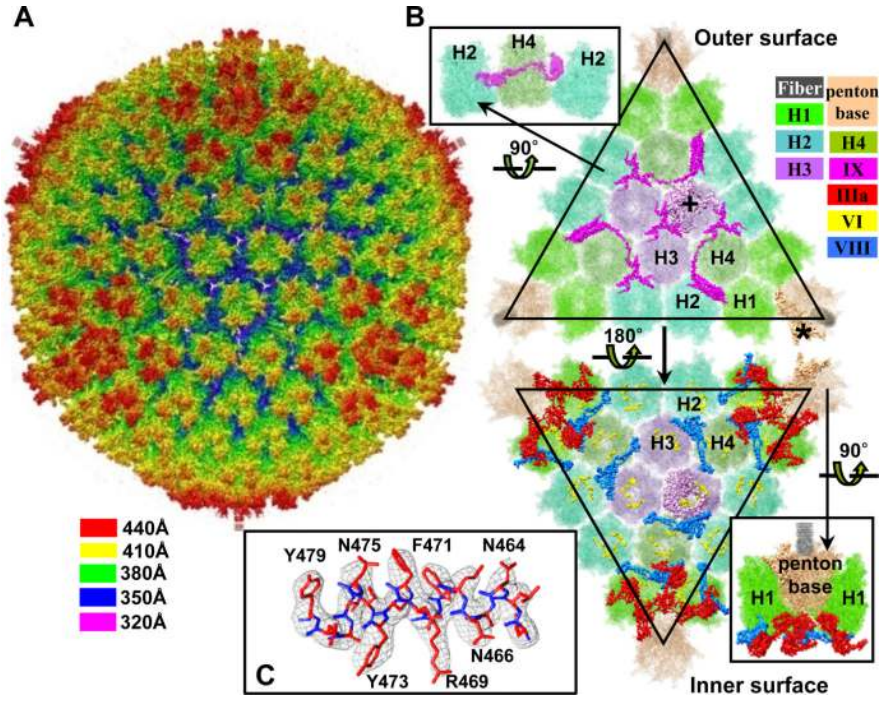

Figure 1.

Overall structure of the Ad5 capsid. (**A**) Radially colored surface of a reconstruction of the capsid, centered on a 3-fold axis. (**B**) Views of the outer surface (upper) showing minor protein IX – and following rotation – the inner surface (lower) of a facet showing minor proteins IIIa, VI, and VIII. All hexons, penton bases, and penton fibers are shown semi-transparently except for one hexon monomer (+) and one penton base monomer (*). Upper left inset: Side view of protein IX among hexons. Lower right inset: Side view of proteins IIIa and VIII centered on a penton base. (**C**) Atomic model (sticks) of an α helix from a hexon monomer superimposed on its density map (mesh) with some side chains labeled.

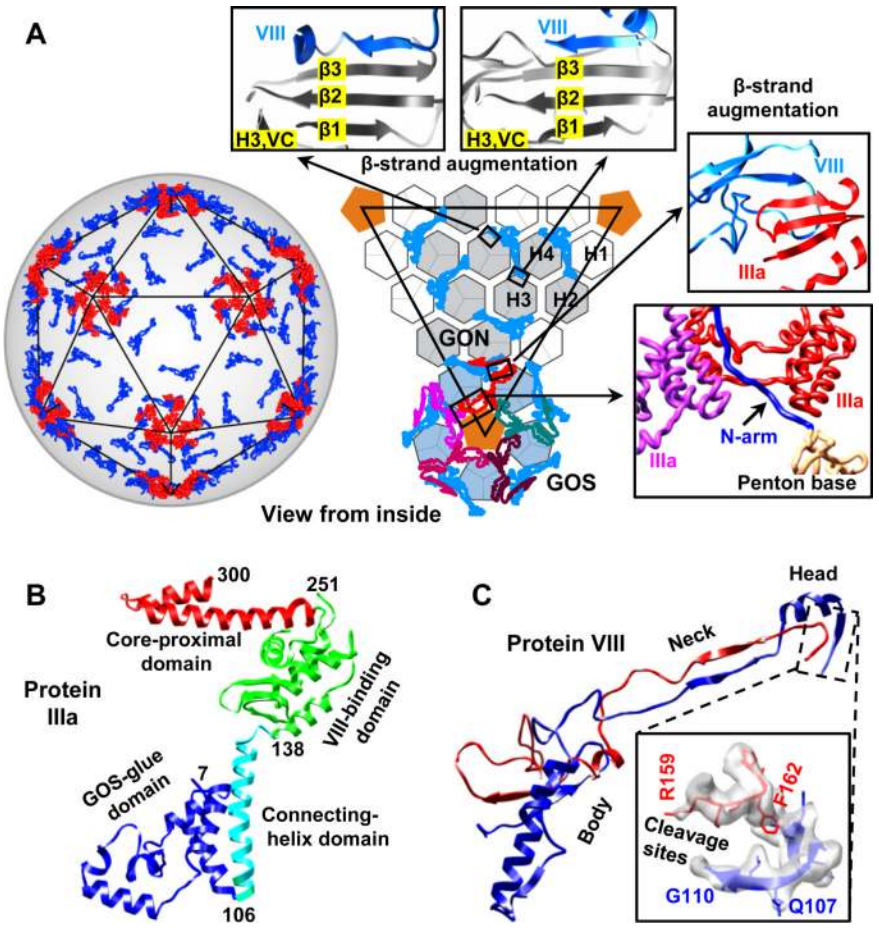

Figure 2.

Interactions among minor and major proteins on the inner surface. (**A**) Left: Global view of the arrangement of protein IIIa (red) and protein VIII (blue). Middle: Organization of hexon trimers into a GON (gray shade), peripentonal hexon trimers (light blue shade) and a penton-base pentamer (orange shade) into a GOS. Top insets: β augmentation at the VC regions of the H3 hexon trimer by the body (left) and the head (right) domains of protein VIII. Right insets: The upper inset shows β augmentation at the VIII-binding domain of protein IIIa by the body domain of protein VIII; the lower inset shows interactions among the N-arm of a penton base and two adjacent proteins IIIa. (**B**) Ribbon model of protein IIIa (aa 7-300) with four domains. (**C**) Ribbon model of protein VIII with three domains. Lower inset: Head domain density (semitransparent gray) and its atomic model (ribbon), showing cleavage sites G110 and R159 between the N-terminal portion (blue) and the C-terminal portion (red).

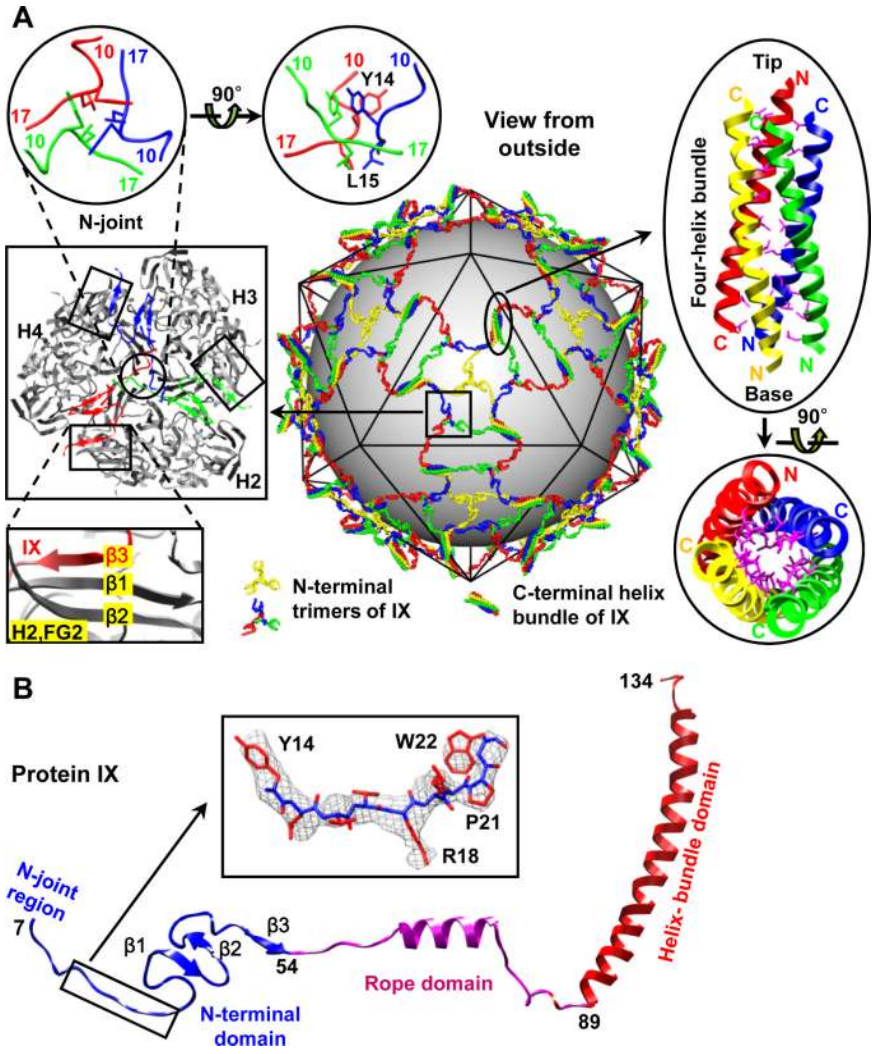

Figure 3.

Interactions among minor and major proteins on the outer surface. (**A**) The physical network of protein IX on the outer surface lashes hexons together into GON tiles but avoids GOS tiles that are each centered on a vertex. Insets: Center left: Ribbon models of the N-terminal domains of three protein IX monomers (blue, green and red), overlying the models of three adjacent hexon (H2, H3, H4) monomers (gray) at a local 3-fold axis. Upper left insets: N-joint of three protein IX monomers and its side view, showing a hydrophobic core containing a triplet of tyrosines (Y14) and a triplet of leucines (L15). Lower left inset: β augmentation at the FG2 region of a hexon H2 by the N termimus of protein IX. Upper right: Four-helix bundle with three parallel and one anti-parallel α helices linked by a ladder of hydrophobic residues (leucines and valines, magenta). Lower right: Head-on view of the helix bundle and the hydrophobic core. (**B**) Ribbon model of protein IX with three domains and the N-joint region. (See also Figure S5.) Inset: Density map (mesh) and atomic model (sticks) of a representative loop from the N-terminal domain.

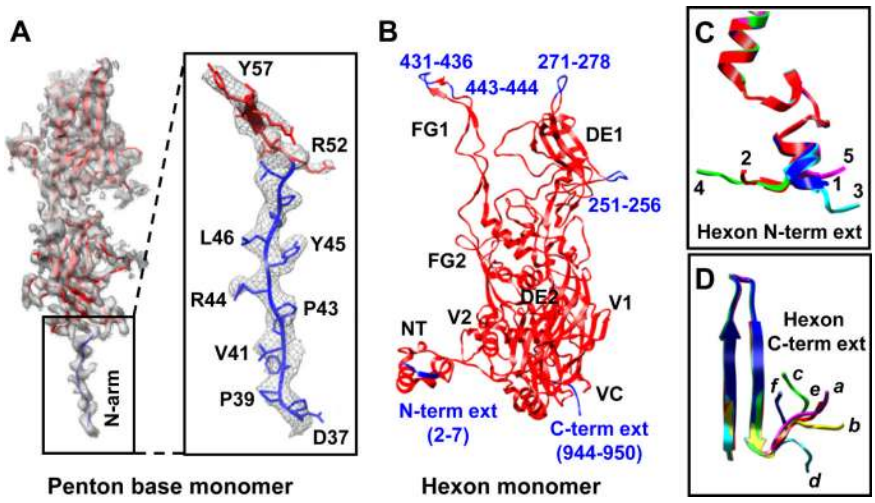

Figure 4.

Newly resolved regions in penton-base and hexon proteins. (**A**) CryoEM model (ribbons) of the penton-base protein superimposed on its density map (semi-transparent gray). Outside the box, the cryoEM atomic model (red ribbons) is identical to the x-ray model (11). Inside the box is our newly resolved N-arm (blue ribbon, aa 37-51). Inset: Enlargement of the boxed region, showing side chain densities (mesh) and its atomic model (ribbon). (**B**) CryoEM model of the hexon protein. Red ribbons show agreement with the x-ray model (10). Blue ribbons show our newly resolved pieces, including the N-terminal and the C-terminal extensions. Region names in the hexon monomer (*e.g.*, VC, FG, *etc.*) follow ref. (10). (**C-D**) Conformational adaptation. (**C**) Twelve hexon monomers exhibit five types of N-terminal extension in an asymmetric unit: four of type 1, two each of types 2 and 3, one of type 4, and three of type 5. (**D**) Twelve hexon monomers exhibit six types of C-terminal extension: two each of types *a, b, c* and *d*, three of type *e*, and one of type *f*. Ribbon models superimposed on density (mesh) of these six types are shown in Fig. S8A.

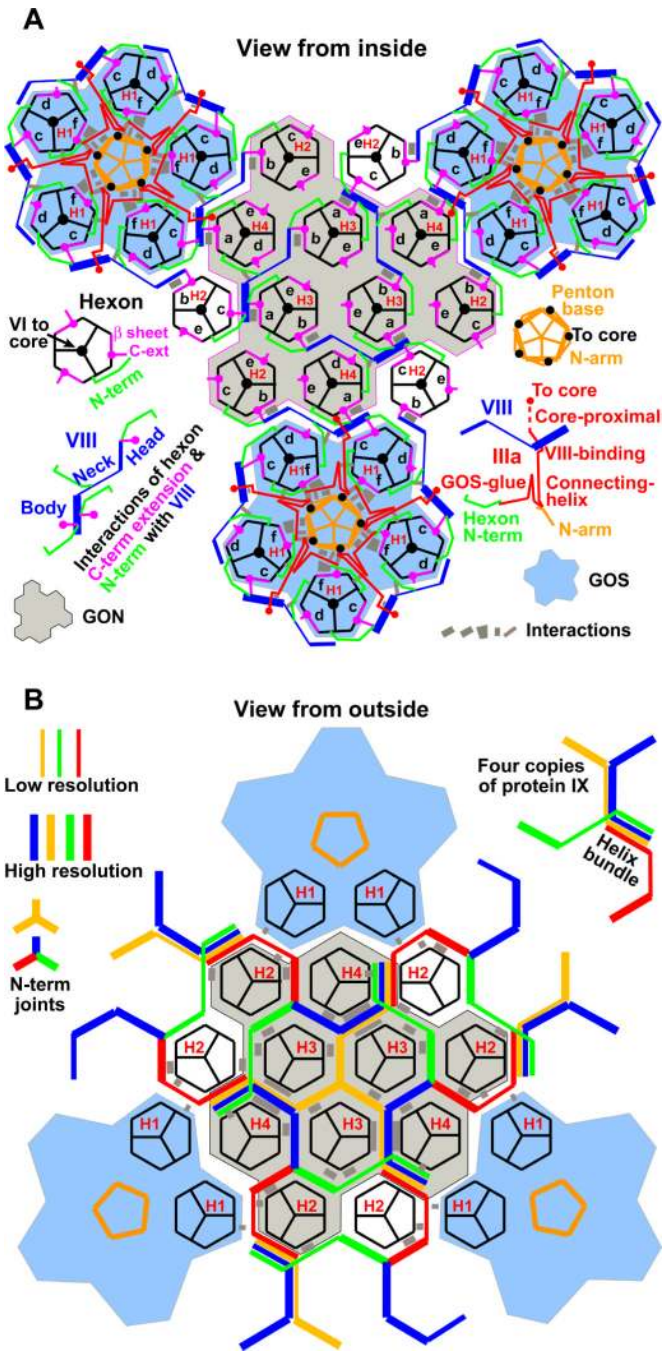

Figure 5.

Schematic illustrations of interactions among minor and major proteins. Interactions are marked here, numbered in Fig. S10, and listed in table S3. (**A**) Contacts on the inner surface of the capsid. Characters a-f denote the positions of six types of hexon C-extensions. At each vertex, five copies of protein IIIa link five peripentonal hexon trimers and a penton-base pentamer to make a GOS tile (light blue shade). Protein VIII mediates binding among hexons, links GON tiles (gray shade) to GON tiles, and links GON tiles to GOS tiles. (**B**) Contacts on the outer surface among the four types of hexon trimer (H1, H2, H3, H4) and the four types of protein IX monomer (red, green, yellow, blue) that are inlaid into the

canyons at the borders between hexons. Protein IX lashes hexons together to form GON tiles and also links GON tiles.